JPE 16-4-23

http://dx.doi.org/10.6113/JPE.2016.16.4.1483
ISSN(Print): 1598-2092 / ISSN(Online): 2093-4718

A Resonant Characteristics Analysis and Suppression Strategy for Multiple Parallel Grid-connected Inverters with LCL Filter

Jian-jun Sun*, Wei Hu†, Hui Zhou*, Yi-ming Jiang*, and Xiao-ming Zha*

*Department of Electrical Engineering, Wuhan University, Wuhan, China
†Grid Center Department, State Grid Hubei Electric Power Research Institute, Wuhan, China

Abstract

Multiple parallel inverters have multiple resonant frequencies that are influenced by many factors. This often results in stability and power quality problems. This paper develops a multiple input multiple output model of grid-connected inverter systems using a closed-loop transfer function. The influence factors of the resonant characteristics are analyzed with the developed model. The analysis results show that the resonant frequency is closely related to the number, type and composition ratio of the parallel inverters. To suppress resonance, a scheme based on virtual impedance is presented, where the virtual impedance is emulated in the vicinity of the resonance frequency. The proposed scheme needs one inverter with virtual impedance control, which reduces the design complexity of the other inverter controllers. Simulation and experimental tests are carried out on two single phase converter-based setups. The results validate the correctness of the model, the analytical results and the resonant suppressing scheme.

Key words: Converters, DC-AC power converters, Modeling, Power electronics, Power system harmonics, Power quality, Resonance

I. INTRODUCTION

Distributed power generation systems have attracted more and more research due to their feasibility and efficiency [1]. As a flexible and efficient grid interface, power electronic converters are widely accepted for connecting renewable energy systems [2]. In the grid-connected mode, an inverter is typically controlled as a current source that injects a certain amount of current into the grid. Most grid-connected inverters are connected in parallel due to the characteristics of current sources.

Due to favorable low-pass filter characteristics, the LCL filter is more widely used to suppress the harmonics around the switching frequency produced by inverter power devices [3], [4]. However, the resonance problem caused by LCL filter making makes it easier for the grid connected inverter to be unstable. As a result, damping solutions are needed. Multiple paralleled inverters connected to a low voltage grid via the point of common connection (PCC) are inter-coupling due to the grid impendence [8]-[10]. Therefore, passive and active solutions for a single LCL inverter model to damp the resonance, which have been studied extensively in [5]-[7] are not variable. Previous studies [11]-[13] show that the resonant behavior of multiple inverters is different from that of a single grid-connected inverter. The authors of [11] established an open-loop transfer function matrix to describe the interaction between parallel inverters. However, the control strategies of inverters are usually MPPT (maximum power point tracking) schemes. Therefore, the transient behavior of resonances cannot be described by this model. An inverter is considered to be an ideal voltage source when analyzing the resonant characteristics of a parallel LCL filter [12]. Without considering the effect of the inverters, a model cannot describe the resonant characteristics between inverters. The discrete domain closed-loop transfer function matrix was established and the resonant characteristics of multiple paralleled inverters were analyzed in [13]. However, the parameters, control strategies and control parameters that

Manuscript received Jul. 24, 2015; accepted Jan. 4, 2016
Recommended for publication by Associate Editor Kyo-Beum Lee.
†Corresponding Author: huweitest@163.com
Tel: +86-027-87562271, Fax: +82-027-87562271, State Grid Hubei Electric Power Research Institute
*Department of Electrical Engineering, Wuhan University, China

directly affect the degree and amount of the resonance frequency are considered to be same. The resonant characteristics of multiple paralleled grid-connected inverters with an LCL Filter are analyzed, but the resonant mechanism and suppression strategy are not studied [14].

Complex resonant characteristics increase the difficulty of harmonic suppression, and seriously affect both the power quality and the system stability. Therefore, this paper develops a multiple input multiple output model of a grid-connected inverter system using a closed-loop transfer function to analyze the system resonance mechanism. In addition, it explores whether the resonance suppression strategy can be successfully applied to applications (such as compressors) where a simple starting control is required [15].

The resonance problem caused by multiple paralleled grid-connected inverters with an LCL filter brings a great challenge to the stability of power systems [16], [17]. In order to improve the capacity of adapting to a weak grid, many passive damping [18] and active damping [19]-[21] methods have been proposed to suppress the resonance of inverters. Active damping methods are widely used in grid-connected inverters, because they can increase structural damping without reducing system efficiency. However, it is difficult to design a damping controller when it is used in multiple paralleled grid-connected inverters which have very complex resonant characteristics and need a high bandwidth [22], [23]. This paper proposes a scheme for changing grid harmonic damping by controlling the harmonic voltage based on an analysis of the resonant characteristics.

In Section II, a transfer function model with multiple-input and multiple-output describing multiple paralleled grid-connected inverters is established based on a Norton model. In Section III, the relationships between the resonant characteristics and the control parameters of the inverters as well as the power grid circumstances are invested. In Section IV, a scheme based on controlling the harmonic voltage to damp the resonant of multiple paralleled grid-connected inverters is proposed. In Section V, an experiment is carried out to verify the analysis of the resonant characteristics and the proposed scheme to damp resonance. Some conclusions are presented in Section VI.

II. Model of Multiple Paralleled Grid-connected Inverters with LCL Filter

Fig. 1 shows the system studied in this paper. Several inverters connected into a grid via the PCC composing a multiple inverter paralleled grid. In this figure, ZL1i and ZL2i are the inverter side and grid side filter impedances, respectively; Z_{Ci} is the filter capacitor; $U_{dc,i}$ is the DC capacitance voltage; and i=1,2,⋯,n is the serial number of the parallel inverters. Lg is the equivalent inductance of the low voltage grid, whose corresponding impedance is Z_g, and u_g is the grid voltage.

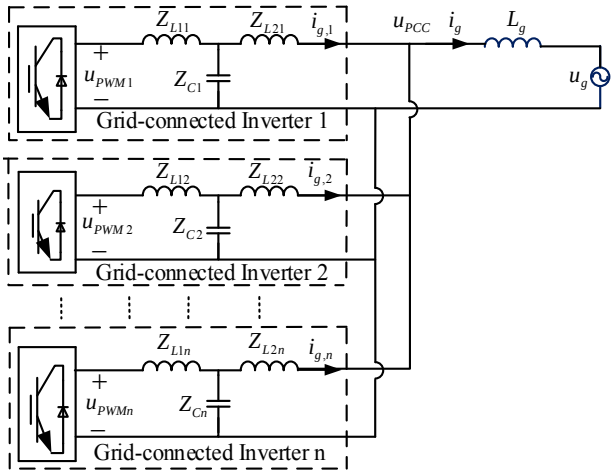

Fig. 1. Block diagram of grid-connected system with multiple LCL inverters.

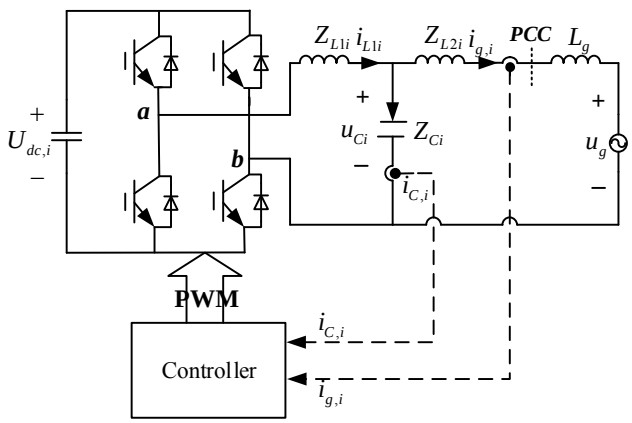

Fig. 2. System structure of single-phase grid-connected inverter with an LCL filter.

Fig. 2 shows the configuration of a grid-connected inverter with an LCL filter. The upper part shows the power circuit while the lower part shows the digital control diagram. The grid currents $i_{g,i}$ and $i_{C,i}$ are current feedbacks to increase damping of the system. A block diagram of the dual-loop control strategy is shown in Fig. 3, where $i_{ref,i}$(s) represents the injected current reference of the outer loop, H_{i1}(s) represent sensor gains of the filter capacitor current, H_{i2} (s) represent the injected current, $G_{t,i}$(s) represents the controller of the outer loop, and G_{inv}(s) represents the gain of the PWM inverter [24]. Applying the equivalent conversion principle to Fig. 3, the equivalent simplified diagram can be obtained as Fig. 4.

The results from the equivalent block diagram are shown in Fig. 4, where:

$$G_{x1}=\frac{G_{t,i}G_{inv,i}Z_{Ci}}{Z_{L1i}+Z_{Ci}+H_{i1}G_{inv,i}}$$
$$G_{x2}=\frac{Z_{Li1}+Z_{iC}+H_{i1}G_{inv,i}}{Z_{L1i}Z_{L2i}+(Z_{L1i}+Z_{L2i})Z_{Ci}+H_{i1}G_{inv,i}Z_{L2i}} \quad (1)$$

The relationship between the input and the output can be

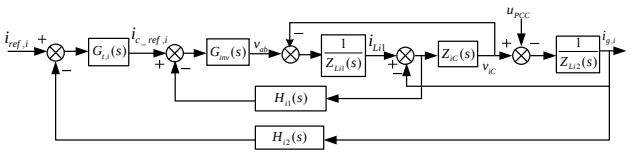

Fig. 3. Block diagram of the dual-loop control strategy of grid-connected inverter.

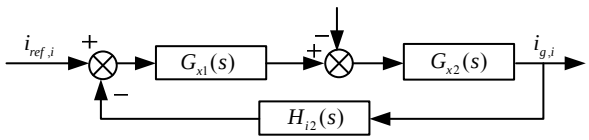

Fig. 4. The equivalent block diagram of the dual-loop control strategy.

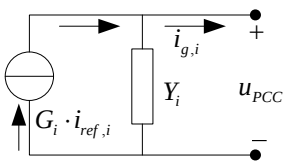

Fig. 5. Norton model of LCL grid-connected inverter control.

expressed as follows:

$$\begin{aligned} i_{g,i} &= \frac{T}{1+T}\frac{1}{H_{i2}} i_{i,ref} - \frac{G_{x2}}{1+T} u_{PCC} \\ &= G_i \cdot i_{i,ref} - Y_i \cdot u_{PCC} \\ &= \frac{G_{i,1}}{G_{i,2}} \cdot i_{i,ref} - \frac{Y_{i,1}}{Y_{i,2}} \cdot u_{PCC} \end{aligned} \tag{2}$$

Where T represents the loop gain of the system, which can be shown as follows:

$$T = G_{x1}G_{x2}H_{i2} = \frac{G_{t,i}G_{inv,i}Z_{Ci}H_{i2}}{Z_{L1i}Z_{L2i} + (Z_{L1i} + Z_{L2i})Z_{Ci} + H_{i1}G_{inv,i}Z_{L2i}} \frac{n!}{r!(n-r)!} \tag{3}$$

According to equation (2), the Norton equivalent circuit shown in Fig. 5 can be established to indicates the external characteristics of grid-connected inverters with LCL filter, were G_i represents the control coefficient of the controlled current source, and Y_i represents the equivalent internal impedance.

Replacing the inverters in Fig. 1 by the Norton equivalent model shown in Fig. 5, the Norton model of multiple paralleled grid-connected inverters with a LCL filter is shown in Fig. 6.

Applying Kirchhoff's law to the circuit, the voltage of the PCC is shown in equation (4).

$$u_{PCC} = \left(\sum_{i=1}^{n} G_i \cdot i_{ref,i} + u_g \cdot Y_g\right) \Big/ \left(\sum_{i=1}^{n} G_i \cdot i_{ref,i} + Y_g\right) \tag{4}$$

From (3) and (4), the current of inverter $i_{g,i}$ can be expressed as:

$$i_{g,i} = R_i \cdot i_{ref,i} + \sum_{t=2}^{n} P_{i,t} \cdot i_{ref,t} - S_i \cdot u_g \tag{5}$$

Where $P_{i,t}$ is the parallel resonance of the inverters t and i; and S_i is the series resonance of the inverter i and the grid. R_i, $P_{i,t}$ and S_i are shown as follows:

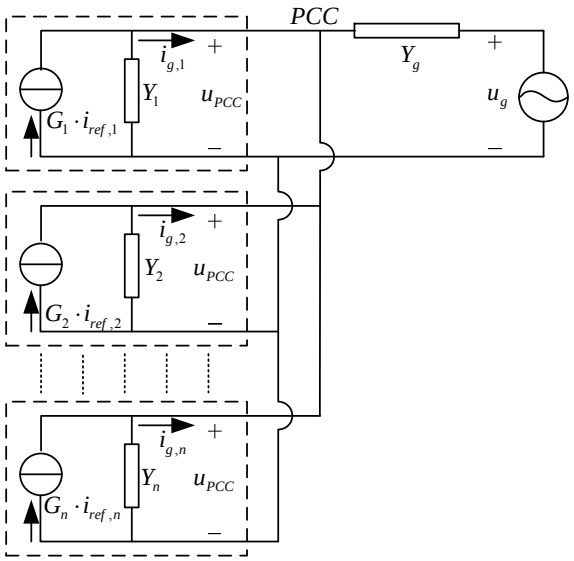

Fig. 6. Norton model of multiple paralleled grid-connected inverters.

$$\begin{aligned} R_i &= \frac{Z_g \cdot \sum_{j=1,j\neq i}^{n} Y_{j,1} \cdot \prod_{k=1,k\neq j}^{n} Y_{k,2} + \prod_{k=1}^{n} Y_{k,2}}{Z_g \cdot \sum_{j=1}^{n} Y_{j,1} \cdot \prod_{k=1,k\neq j}^{n} Y_{k,2} + \prod_{k=1}^{n} Y_{k,2}} \cdot \frac{G_{i,1}}{G_{i,2}} \\ P_{i,t} &= \frac{-Z_g \cdot Y_{i,1} \cdot \prod_{j=1,j\neq i}^{n} Y_{j,2}}{Z_g \cdot \sum_{j=1}^{n} Y_{j,1} \cdot \prod_{k=1,k\neq j}^{n} Y_{k,2} + \prod_{k=1}^{n} Y_{k,2}} \cdot \frac{G_{i,1}}{G_{i,2}}; t \neq i \\ S_i &= \frac{Z_g \cdot Y_{1,i} \cdot \prod_{j=1,j\neq i}^{n} Y_{j,2}}{Z_g \cdot \sum_{j=1}^{n} Y_{j,1} \cdot \prod_{k=1,k\neq j}^{n} Y_{k,2} + \prod_{k=1}^{n} Y_{k,2}} \end{aligned} \tag{6}$$

Where G_i=G_{i1}/G_{i2}. Equation (7) describes the current of multiple paralleled grid-connected inverters.

$$\begin{pmatrix} i_{g,1} \\ i_{g,2} \\ \cdots \\ i_{g,n} \end{pmatrix} = \begin{pmatrix} R_1 & P_{12} & \cdots & P_{1n} \\ P_{21} & R_2 & \cdots & \cdots \\ \cdots & \cdots & \cdots & \cdots \\ P_{n1} & P_{n2} & \cdots & R_n \end{pmatrix} \cdot \begin{pmatrix} i_{ref,1} \\ i_{ref,2} \\ \cdots \\ i_{ref,n} \end{pmatrix} - \begin{pmatrix} S_1 \\ S_2 \\ \cdots \\ S_n \end{pmatrix} \cdot u_g \,. \tag{7}$$

As can be seen from equation (7), the nonzero impedance of a low voltage grid causes the coupling between parallel inverters. Moreover, the resonant characteristics are more complicated because of this interaction.

III. Resonant Characteristics Analysis

To determine how the numbers, types and composition ratios of parallel inverters affect the resonant characteristics, this paper studied three inverters A, B and C. Inverters using the same dual-loop control strategy but with different parameters are shown in Table I. The inverters are connected to a weak grid through the PCC. The grid voltage is 220V and the frequency is 50Hz. The equivalent inductance and resistance of the power grid are set to 1.5mH and 0.05Ω, respectively, based on the relationship between the SCR and the equivalent impedance of the power grid [25]. The zeros and poles of R_i, $P_{i,t}$ and S_i are the same. As a result, analyzing only R_i can fully describe the resonant characteristics.

TABLE I
PARAMETERS OF INVERTER A, B AND C

Paramenters / Inverter	L_1(mH)	R_1(Ω)	L_2(mH)	R_2(Ω)	C(uF)	K_p	K_r	H_{i1}	H_{i2}	U_{dc}(V)
A	4	0.25	0.5	0.05	40	1	200	0.2	0.2	500
B	1	0.1	0.2	0.05	20	0.6	300	0.1	0.2	500
C	3	0.2	0.6	0.06	30	1	100	0.4	0.2	500

TABLE II
THE COMPOSITION RATIO OF INVERTERS

	ratio	1	2	3	4
Case I	A/C	1:5	2:4	3:3	4:2
Case II	A/B/C	1:4:1	2:3:1	3:2:1	4:1:1

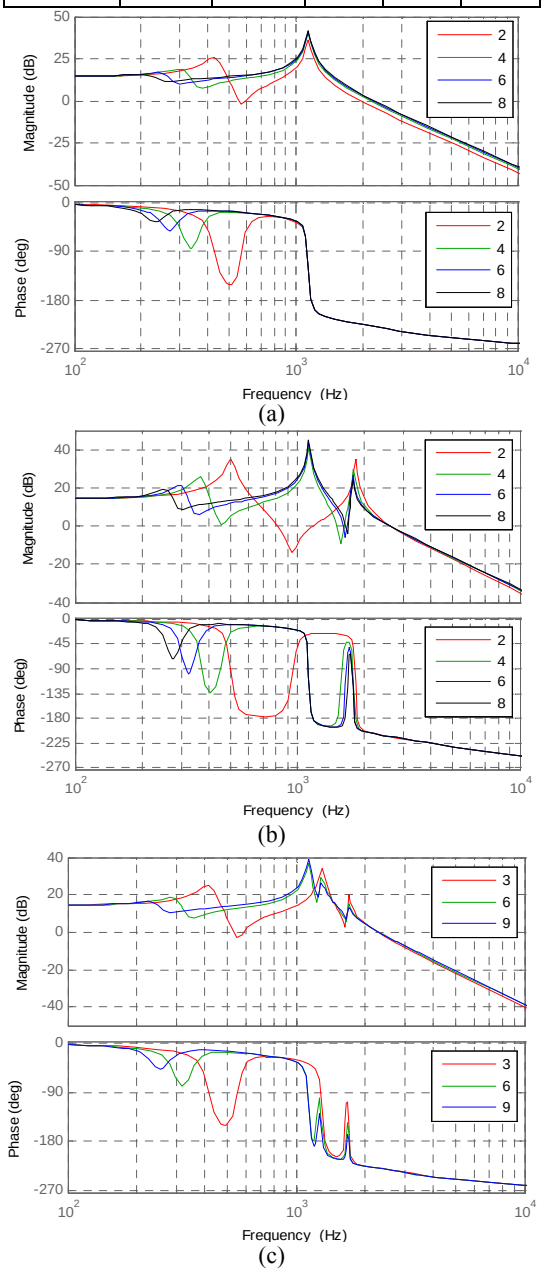

Fig. 7. The resonant characteristics of different grid-connected inverter number.

A. The Number of Paralleled Grid-Connected Inverters

Fig. 7(a), (b) and (c) indicate how the number of grid-connected inverters with an LCL filter affects the resonant characteristics. The lines with different colors represent the number of the paralleled inverters. Fig. 7(a) shows that all of the paralleled inverters are A; Fig. 7(b) shows that the composition ratio of inverters A and B is 1:1; Fig. 7(c) shows that the composition ratio of inverters A, B and C is 1:1:1. The total number of paralleled inverters is shown on the top right corner.

Multiple positive resonant peaks are shown in Fig. 7 when multiple inverters are paralleled into a grid. The lower resonant frequency increases with a decreasing number of parallel inverters, and the type of inverters affects the number of resonant peaks. When the composition ratio of the inverters is fixed, the resonant peak is stable without the effect of parallel inverter number.

This paper analyzed a grid connecting six inverters in two cases. Case I: inverters A and C compose the parallel inverter system. Case II: inverters A, B and C compose the parallel inverter system. Table II shows the composition ratio of these six inverters. Fig. 8(a) and (b) show the resonant characteristics analysis results, in which the colored lines represent the ratios of the inverters as defined in Table II. Fig. 8 indicates that the composition ratios and types of the inverters have great effects on the resonance frequency and quantity.

B. The Effect of Parameters on the Resonant Characteristics

The control parameters and the strength of the grid are factors that greatly affect the resonant characteristics of multiple paralleled grid-connected inverters. The parameters for the sensor gain (H_{i1}), the outer current loop control (K_p) and (K_i), and the grid strength (L_g) are considered in this paper. Fig. 9 show the relationship between the resonant characteristics and the parameters, in the case of a system composed of inverter A and B. Fig. 9(a), (b), (c) and (d) show the effects of the sensor gain (H_{i1}), (K_p), (K_i), and the grid strength (L_g), respectively.

As can be seen from Fig. 9(a), the resonant frequency increases as the sensor gain H_{i1} decreases. Fig. 9(b) shows that the resonant frequency decreases as the control parameter of K_p decreases. Fig. 9(c) indicates that the control parameter K_i affects the resonant peak, but has no effect on the resonant

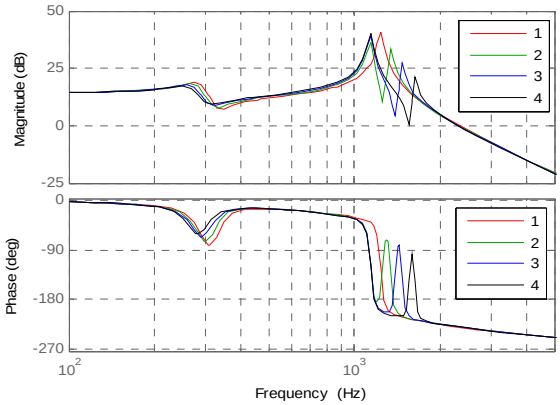

(a)

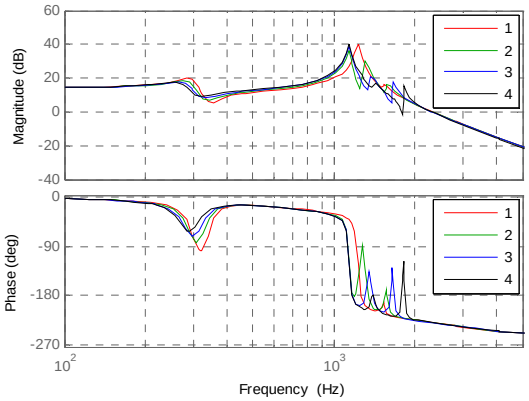

(b)

Fig. 8. Resonance characteristics of six paralleled grid-connected inverters. (a) case I. (b) case II.

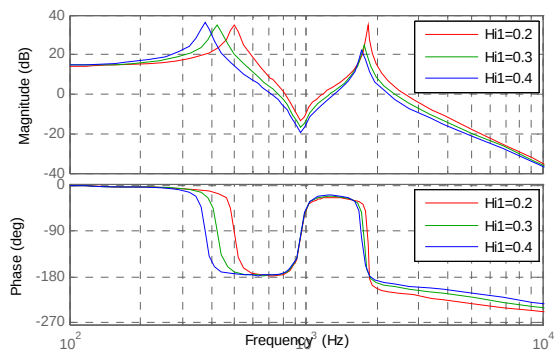

(a)

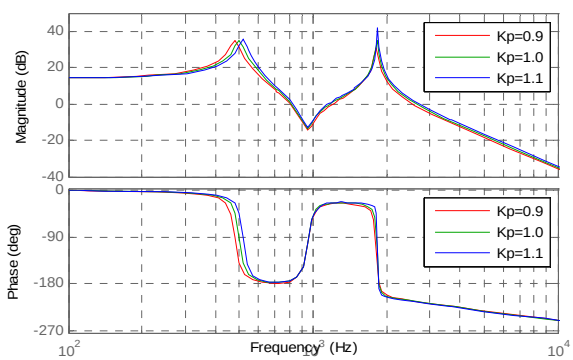

(b)

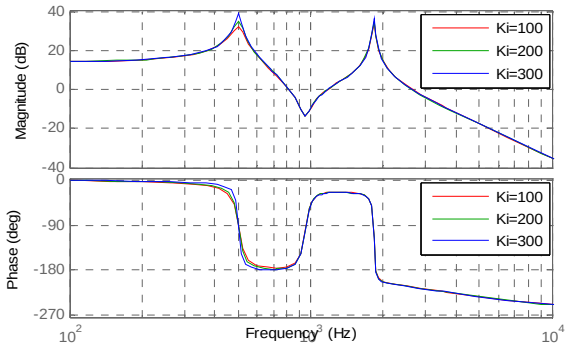

(c)

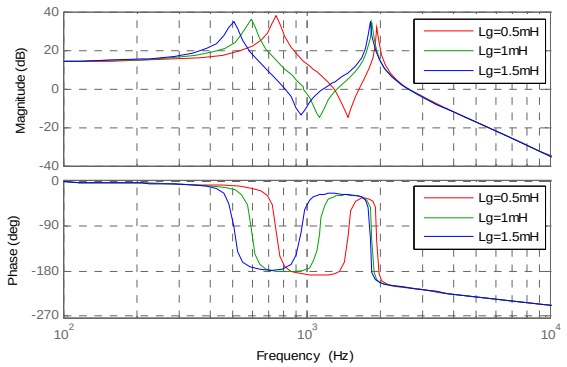

(d)

Fig. 9. Influence of the parameters to the resonant characteristics. (a) H_{i1}. (b) K_p. (c)K_i.(d) grid impedance.

frequency. Fig. 9(d) demonstrates that with the enhancement of the power grid strength, the resonant frequency increases.

IV. SCHEME FOR RESONANT SUPPRESSION

The above research shows that the resonant characteristics are influenced by the number of inverters and their control parameters. To suppress resonance, the damping of a system should be enhanced. Active damping can be realized by impendence reshaping using the voltage of the PCC. However, there are several resonant frequencies in a multiple inverter system, and the resonant frequency changes as the working conditions shift. Therefore, a high bandwidth damping controller is needed in order to cover a wide range of resonant frequencies. This introduces difficulty to the design of the damping controller.

It can be shown from the above analysis that resonance is caused by grid impendence. Therefore, this resonance can be suppressed by reshaping the impedance of the grid. A global suppression strategy based on virtual admittance is proposed to solve the resonance problem. The equivalent circuit of a system with virtual admittance is shown in Fig. 10.

With virtual admittance, the grid current of the inverter i can be expressed as follows:

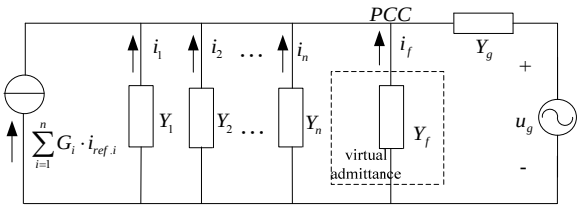

Fig. 10. Equivalent circuit of system with virtual admittance.

$$i_{g.i} = G_i \cdot i_{ref.i} - \sum_{k=1}^{n}(G_k \cdot i_{ref.k}) \cdot \frac{Y_i}{L+Y_f} - u_g \cdot \frac{Y_g \cdot Y_i}{L+Y_f}$$
$$= G_i \cdot i_{ref.i} - \sum_{k=1}^{n}(G_k \cdot i_{ref.k}) \cdot M_i^* - u_g \cdot N_i^* \quad (8)$$

where: $L = \sum_{k=1}^{n} Y_k + Y_g$; $M_i^* = \frac{Y_i}{L+Y_f}$; $N_i^* = \frac{Y_g \cdot Y_i}{L+Y_f}$

To suppress the resonance of a system and to guarantee that the fundamental wave control is not affected, the virtual admittance Y_f near the resonance frequency should be much larger than L to minimize M_i^* and N_i^*, while Y_f should be much smaller than L at other frequencies, which does not affect the control under this frequency. Considering that a band-pass filter has a very large gain at the pass-band frequency, while it has a very small gain at other frequencies, a second order band-pass should be chosen as the virtual admittance. The transfer function of Y_f is as follows:

$$Y_f = H = A\frac{s(\omega_0/Q)}{s^2 + s(\omega_0/Q) + \omega_0^2} \quad (9)$$

ω 0 and Q denote the resonance frequency and the bandwidth of the filter, respectively. A control block can be embed in a inverter if its power rating is high enough or if another converter without active power control can be used to achieve the control.

Therefore, the impedance of the grid can be reshaped by controlling the resonant voltage of the PCC to suppress resonance. The resonant voltage compensation scheme is shown in Fig. 11. Since only one controller is needed to control the resonance voltage of the PCC, the burden of the other controllers is reduced. As a result, their performances are improved. Simulation and experimental results of the proposed scheme will be presented in section V.

V. Simulation and Experimental Results

A. Simulation Results of the Resonant Characteristics

A MATLAB/Simulink electromagnetic transient model of a micro-grid composing two paralleled grid-connected inverters is established to verify the analysis results. As can be seen from Fig. 7(a) and Fig. 7(b), the resonance frequency of a two grid-connected inverter system consisting of A is 420Hz and one consisting of A and B is 490Hz. Therefore, a 5% harmonic of 400Hz was injected into inverter A when the system consisted of A, while a 5% harmonic of 500Hz was

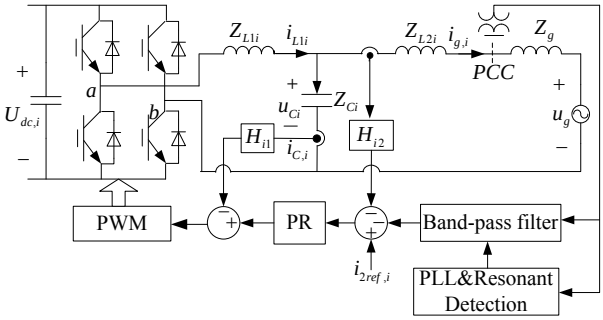

Fig. 11. Control Block Diagram of the resonant compensation scheme.

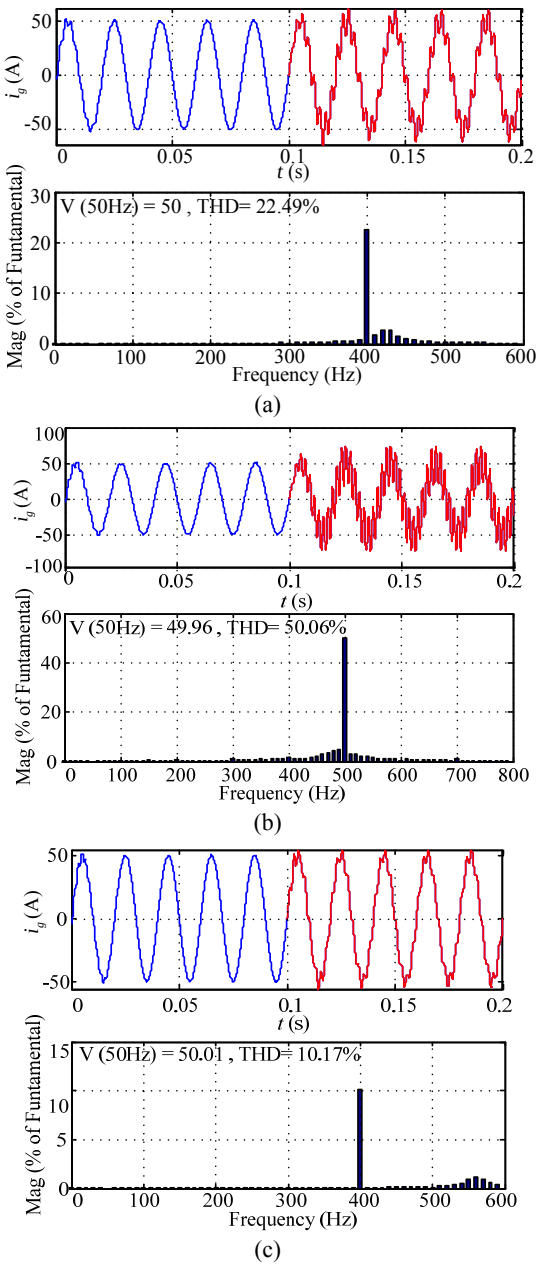

Fig. 12 The Current and its THD of grid-connected inverter A. (a) two grid-connected inverters consisted A. (b) grid-connected inverters consisted A and B. (c) only inverter A connected to grid.

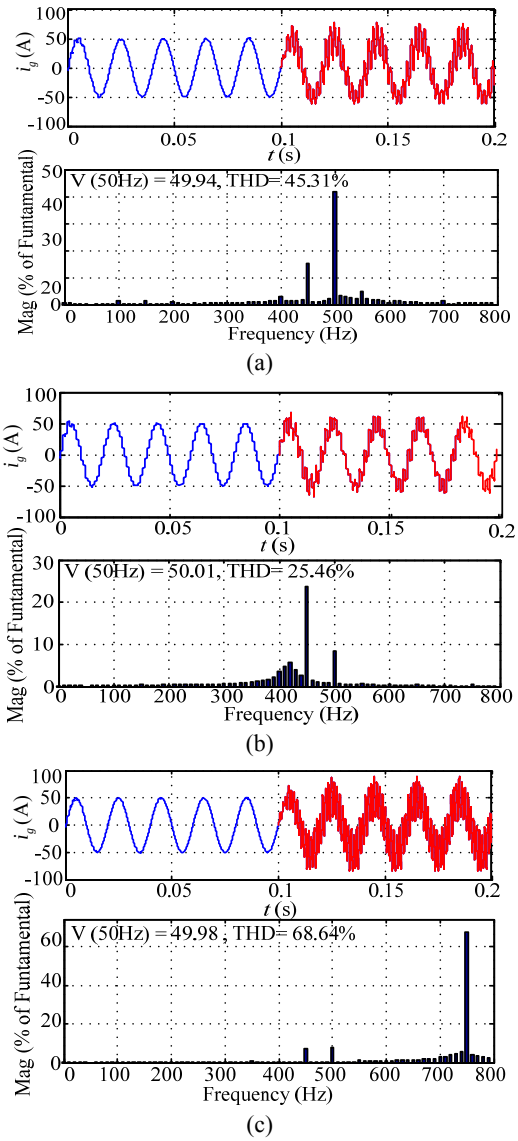

Fig. 13. The current and its THD of grid-connected inverter A. (a) H_{i1}=0.2 and L_g=1.5mH. (b) H_{i1}=0.3 and L_g=1.5mH. (c) H_{i1}=0.2 and L_g=0.5mH.

injected into inverter A when the system consisted of A and B, considering that the harmonic frequency is an integral multiple of the fundamental frequency (50Hz). The equivalent inductance and resistance of the power grid are stetted to 1.5mH and 0.05Ω, respectively. The simulation parameters of inverters A and B are shown in Table I.

The current of inverter A and its THD are shown in Fig. 11. Where (a) represents two inverters composed of A connecting to the grid, (b) represents two inverters composed of A and B connecting to the grid, and (c) represents only one inverter A connecting to the grid.

It can be seen that the 400Hz harmonic is enlarged by comparing Fig. 12(a) and Fig. 12(c). In other words, the inherent resonance frequency of an LCL filter is added by a lower resonant frequency when two inverters are connected to the PCC. The resonant frequency and peaks are closely

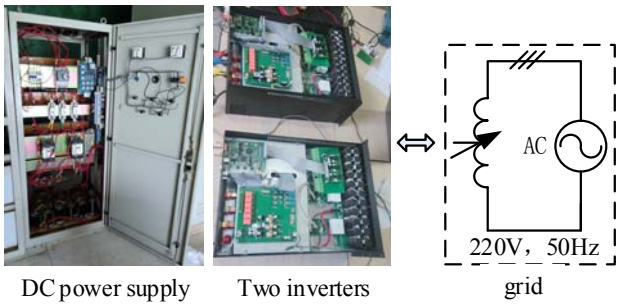

Fig. 14. The inverter and experiment platform used in the experiment.

related to the type of inverter, as given in a comparison of Fig. 12(a) and Fig. 12(b). The effectiveness of the proposed analysis method is demonstrated by the consistency of the simulation results and theoretical analysis.

As can be seen in Fig. 10(a) and (d), the resonant characteristics are mainly influenced by H_{i1} and L_g. Therefore, only the influence of these two parameters is analyzed. A simulation is executed with a two grid-connected inverter system. The first converter has parameters that are similar to those of inverter A, as shown in Table 1, except that H_{i1} and L_g are different. In addition, the second inverter has the same parameters as those of inverter B, as can be seen in Table 1. When a 5% harmonic of 400Hz, 500Hz and 750Hz was injected into the first inverter, the current of inverter B and its THD are shown in Fig. 13(a), (b) and (c). Fig. 13(a) represents the situation where H_{i1}=0.2 and L_g=1.5mH, (b) represents the situation where H_{i1}=0.3 and L_g=1.5mH, and (c) represents the situation where H_{i1}=0.2 and L_g=0.5mH.

It can be seen that the resonant frequency decreases as the sensor gain Hi1 increases by comparing Fig. 13(a) and Fig. 13(b), which verifies the correctness of the analysis results in Fig. 9(a). A comparison of the results of Fig. 13(a) and Fig. 13(c) show that the resonant frequency increases as the grid impedance decreases, which validate the correctness of the analysis results in Fig. 10(d).

B. Experiment Results of the Resonant Characteristics

Experiments have been carried out to verify the theoretical analysis. Fig.14 shows the converters and experimental platform used in the experiments. The experiments have been carried on two eight-cell cascaded converters, where one cell was reconstructed for this experiment. A digital signal processor (TMS320F2812) and a field programmable gate array (EP2C50F484C8) compose the central controller. Three-phase diode rectifiers are used to provide the dc link voltages for these inverters. A reactor is used to enlarge the equivalent impedance of the grid.

The experiments were conducted under the same conditions as the simulation. A 5% harmonic of 400Hz was injected into inverter A when the system consisted of A, while a 5% harmonic of 500Hz was injected into inverter A when the system consisted of A and B. The equivalent

TABLE III
PARAMETERS OF INVERTER D AND E USED IN EXPERIMENT

Parameters \ Inverter	Inverter A	Inverter B
L_1(mH)	4	1
R_1(Ω)	0.25	0.1
L_2(mH)	0.5	0.2
R_2(Ω)	0.05	0.05
C(uF)	40	20
K_p	0.8	0.7
K_r	100	200
H_{i1}	0.15	0.1
H_{i2}	0.2	0.1
U_{dc}(V)	500	500
Switch Frequency(Hz)	12.8k	12.8k
Samping Frequency	25.6k	25.6k
Rated Power(kW)	15	20

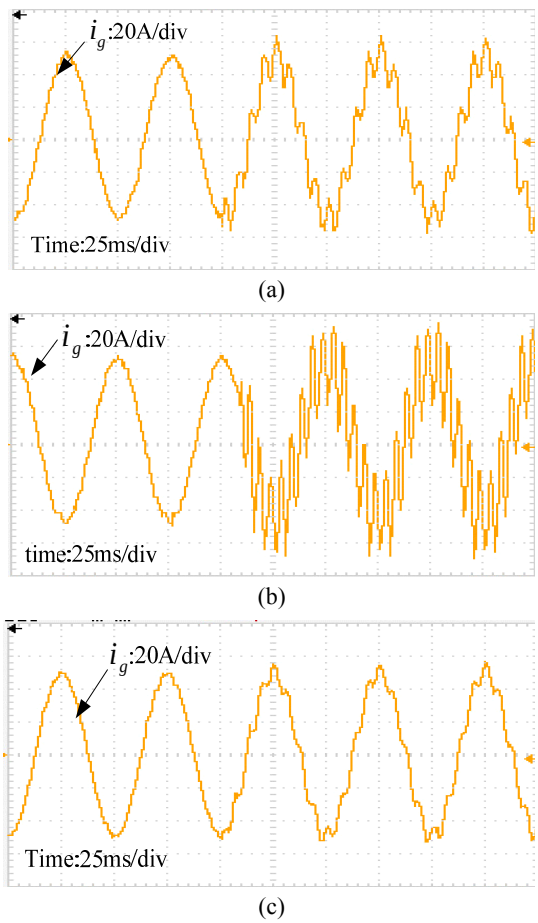

Fig. 15. The current of grid-connected inverter A. (a) two grid-connected inverters consisted A. (b) grid-connected inverters consisted A and B. (c) only inverter A connected to grid.

inductance 15mH and resistance 0.05Ω were simulated through a series reactor to decrease the strength of the grid. The filter parameters of the inverter used in the experiment

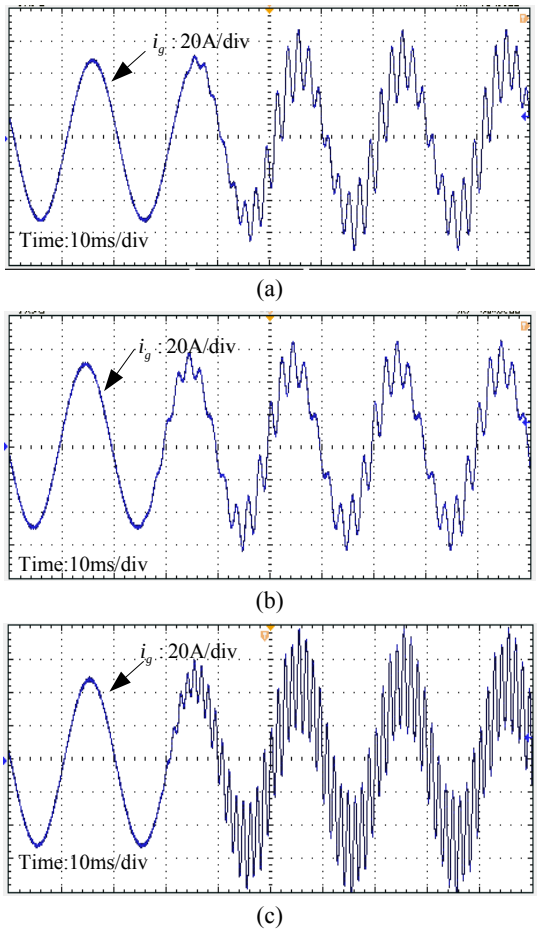

Fig. 16 The Current of grid-connected inverter A. (a) H_{i1}=0.2 and L_g=1.5mH. (b) H_{i1}=0.3 and L_g=1.5mH. (c) H_{i1}=0.2 and L_g=0.5mH.

are same as those used in the simulation, while the parameters for the system damping are different from those used in the simulation. Therefore, in order to obtain the same resonant frequency, the control parameters need to be different from the simulation. The experiment parameters of inverter A and B are shown in Table III.

The current of grid-connected inverter A is shown in Fig. 15(a), (b) and (c). Fig. 15(a) represents two inverter A connecting to the grid. Fig. 15(b) represents two inverter A and B connecting to the grid. Fig. 15(c) represents only one inverter A connecting to the grid.

A comparison of Fig.12 and Fig.15 shows that the two parallel grid-connected converter system add a lower resonant frequency into the inherent resonance frequency of the LCL filter. It can also be seen that the type of the inverters has great effect on the resonant frequencies, which matches with the frequency domain analysis in Fig. 7(a) and (b).

An experiment is carried out with the two grid-connected inverter systems. The experimental conditions are the same as those for the simulation executed above. A 5% harmonic of 400Hz, 500Hz and 750Hz was injected into the first inverter.

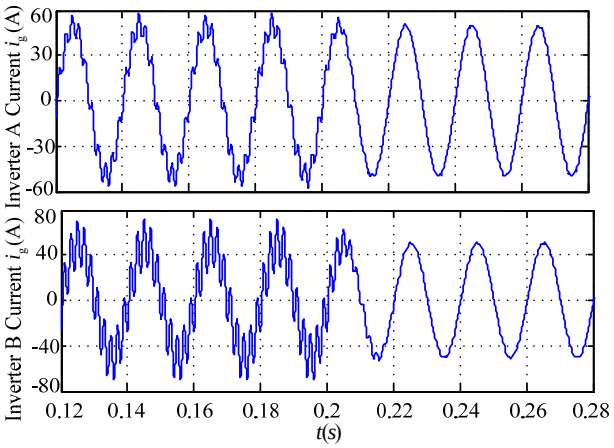

Fig. 17. Simulated currents waveform of inverter B before and after applying the harmonic suppression strategy.

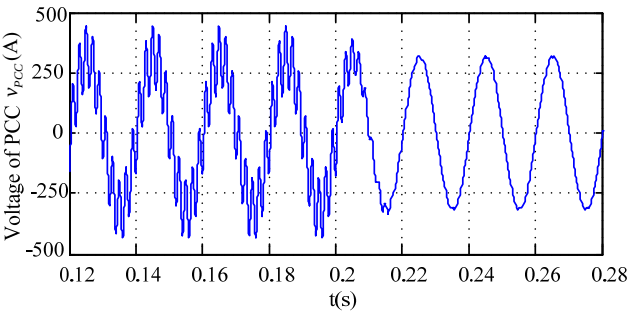

Fig. 18. Simulated voltage waveform of PCC without and with applying the harmonic suppression strategy.

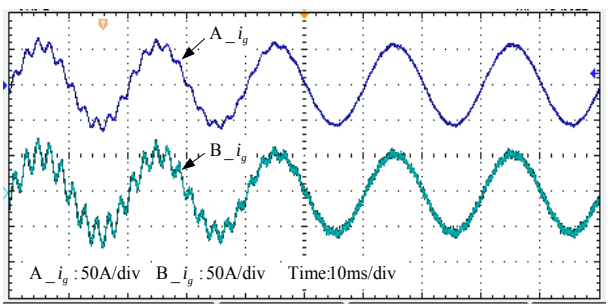

Fig. 19. Simulated currents waveform of inverter B before and after applying the harmonic suppression strategy.

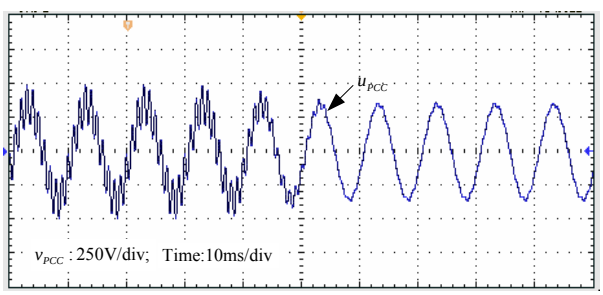

Fig. 20. Simulated voltage waveform of PCC without and with applying the harmonic suppression strategy.

The current and its THD are shown separately in Fig. 17(a), (b) and (c). Fig. 17(a) represents the situation where H_{i1}=0.2 and L_g=1.5mH, (b) represents the situation where H_{i1}=0.3 and L_g =1.5mH, and (c) represents the situation where H_{i1}=0.2 and Lg =0.5mH.

A comparison of Fig. 13 and Fig. 16 illustrates that the resonance frequency of the multiple parallel inverter system is related to the control parameters and grid strength, which is in accordance with the analysis results of Fig. 10.

C. Simulation Results of the Resonant Suppression

Corresponding to the analysis currents shown in Fig. 7(b), the two grid-connected inverters consist of A and B, and a 5% harmonic 500Hz is injected, where the setting value of inverter A at 0.1s. Meanwhile, inverter B uses the harmonic suppression strategy shown in Fig.10 at 0.2s. The equivalent inductance and resistance of the power grid are preferable to 1.5mH and 0.05Ω, respectively.

Fig. 17 shows simulated current waveforms of the inverters before and after applying the harmonic suppression strategy at 0.2s. The simulations shown in Fig. 17 indicate that the resonance caused by the dynamic interactions between the control loops of the paralleled inverters is stabilized by the harmonic suppression strategy. Fig. 18 shows the change of the PCC voltage once the harmonic suppression strategy is enabled at the instant of 0.2s. An effective resonance damping of the PCC voltage can be observed.

D. Experiment Results of the Resonant Suppression

The experimental platform is shown in Fig. 14. The experimental and simulation conditions are the same, while the control parameters used in experiment are different from those used in the simulation to obtain the same resonant frequency.

Fig. 19 shows the measured output currents of the inverters before and after applying the scheme for resonant suppression. In addition, the measured PCC voltage waveform in this case is shown in Fig. 20. The experimental results show that the resonance can be suppressed by controlling the harmonic voltage of the PCC completed by one inverter. This simplifies the design of the other damping controllers.

VI. CONCLUSIONS

A model of multiple paralleled grid-connected inverters with a LCL filter has been established in this paper. The resonant characteristics have been theoretically analyzed based on this model, which indicates that there is more than one resonant frequency when multiple inverters are paralleled into grid, and that the number, type and composition ratio of the parallel inverters greatly affect the resonant frequency. In addition, the lower resonance frequency increases with a decreasing number of parallel inverters, and the control parameters and the grid strength are the main effect factors when the number of inverters is fixed. The method for implementing the direct resonant voltage compensation on only one inverter simplifies the design of the other damping controllers. The capability of the model and the accuracy of

the analytical results are verified by time-domain simulation and experimental results and the effectiveness of the resonant suppressing scheme.

ACKNOWLEDGMENT

Project Sponsored by National Natural Science Foundation of China. (51190102, 51277137 and 51177113).

REFERENCES

[1] F. Blaabjerg, R. Teodorescu, and M. Liserre, "Overview of control and grid synchronization for distributed power generation systems," *IEEE Trans. Ind. Electron.*, Vol. 53, No. 5, pp. 1398-1409, Oct. 2006.

[2] J. M. Carrasco, L. G. Franquelo, J. T. Bialasiewwicz, E. Galvan, R. C. P. Guisado, M. A. M. Prats, J. I. Leon, and N. Moreno-Alfonso, "Power electronic systems for the grid integration of renewable energy sources: A survey," *IEEE Trans. Ind. Electron.*, Vol. 53, No. 4, pp. 1002-1016, Aug. 2006.

[3] M. Liserre, F. Blaabjerg, and S. Hansen, "Design and control of an LCL filter based three-phase active rectifier," *IEEE Trans. Ind. Appl.*, Vol. 41, No. 5, pp. 1281-1291, Sep./Oct. 2005.

[4] K. Jalili and S. Bernet, "Design of LCL filters of active-front-end two level voltage-source converters," *IEEE Trans. Ind. Electron.*, Vol. 56, No. 5, pp. 1674-1689, May 2009.

[5] J. Dannehl, F. W. Fuchs, and S. Hansen, and P. B. Thogersen, "Investigation of active damping approaches for PI-based current control of grid-connected pulse width modulation converters with LCL filters," *IEEE Trans. Ind. Electron.*, Vol. 46, No. 4, pp. 1509-1517, Jan. 2010.

[6] J. R. Massing, M. Stefanello, H. A. Gründling, and H. Pinheiro, "Adaptive current control for grid-connected converters with LCL filters," *IEEE Trans. Ind. Electron.*, Vol. 59, No.11, pp. 4681-4693, Dec. 2012.

[7] M. Malinowski and S. Bernet, "A simple voltage sensorless active damping scheme for three-phase PWM converters with an LCL filter," *IEEE Trans. Ind. Electron.*, Vol. 55, No. 4, pp. 1876-1880, Apr. 2008.

[8] J. H. R. Enslin and P. J.M. Heskes, "Harmonic interaction between a large number of distributed power inverters and the distribute network," *IEEE Trans. Power Electron.*, Vol. 19, No. 6, pp. 1586-1593, Nov. 2004.

[9] F. Wang, J. L Duarte, M. A. M. Hendrix, and P. F. Ribeiro, "Modeling and analysis of grid harmonic distortion impact of aggregated DG inverters," *IEEE Trans. Power Electron.*, Vol. 26, No. 3, pp. 786-797, Mar. 2011.

[10] D. Zh. Xu, F. Wang, H. L. Mao, Y. Ruan, and W. Zhang. "Modeling and Analysis of Harmonic Interaction Between Multiple Grid-connected Inverters and the Utility Grid," *Proceedings of the CSEE*, Vol. 33, No. 12, pp. 64-71, Apr. 2013.

[11] J. Agorreta, M. Borrega, J. Lopez, and L. Marroyo, "Modeling and control of N paralleled grid-connected inverters with LCL filters coupled due to grid impedance in PV plants," *IEEE Trans. Power Electron.*, Vol. 26, No. 3, pp. 700-785, Apr. 2011.

[12] X. N. Lu, K. Sun, and L. P. Huang, "Resonance characteristics in a parallel LCL filter system for microgrid applications," Tsinghua Univ. (Sci &. Tech), Vol. 52, No. 11, pp. 1571-1577, Nov. 2012.

[13] J. W. He, "Investigation and active damping of multiple resonances in a parallel-inverter-based microgrid," *IEEE Trans. Power Electron.*, Vol. 28, No. 1, pp. 234-246, Jan. 2013.

[14] W. Hu, J. J. Sun, Q. Ma, C. Yin, F. Liu, and X. Zha, "Modeling and resonant characteristics analysis of multiple paralleled grid-connected inverters with LCL filter," *IEEE Energy Conversion Congress and Exposition*, pp. 3371-3377, 2014.

[15] J. Sun, "Impedance-based stability criterion for grid-connected converters," *IEEE Trans. Power Electron.,* Vol. 26, No. 11, pp. 3075-3078, Nov. 2011.

[16] J. Yin, S. Duan, and B. Liu, "Stability analysis of grid-connected inverter with LCL filter adopting a digital single-loop controller with inherent damping characteristic," *IEEE Trans. Ind. Informat.*, Vol. 9, No. 2, pp. 1104-1112, May 2013.

[17] S. Vesti, T. Suntio, J. A. Oliver, R. Prieto, and J. A. Cobos, "Impedance based stability and transient-performance assessment applying maximum peak criteria," *IEEE Trans. Power Electron.*, Vol. 28, No. 5, pp. 2099-2104, May 2013.

[18] M. Liserre, F. Blaabjerg, and S. Hansen, "Design and control of an LCL-filter based active rectifier," IEEE Trans. Ind. Appl., Vol. 41, No. 2, pp. 1281-1291, Sep./Oct. 2005.

[19] E. Twining amd D. Holmes, "Grid current regulation of a three phase voltage source inverter with an LCL input filter," *IEEE Trans. Power Electron.*, Vol.18, No.3, pp.888-895, May 2003.

[20] M. Malinowski and S. Bernet, "A simple voltage sensorless active damping scheme for three-phase PWM converters with an LCL filter," *IEEE Trans. Ind. Electron.*, Vol. 55, No. 4, pp. 1876-1880, Apr. 2008.

[21] X. h. Zhou, J.W. Fan, and A. Q. Huang, "High-frequency resonance mitigation for plug-in hybrid electric vehicles' integration with a wide range of grid conditions," *IEEE Trans. Power Electron.*, Vol. 27, No. 11, pp. 4459-4471, Nov. 2012.

[22] X. F. Wang, F. Blaabjerg, and M. Liserre, "An active damper for stabilizing power-electronics-based AC systems," *IEEE Trans. Power Electron.*, Vol. 29, No. 7, pp. 3318-3329, Jul. 2014.

[23] X. F. Wang, F. Blaabjerg, and M. Liserre, "An active damper to suppress multiple resonance with unknown frequencies," *Applied Power Electronics Conference and Exposition (APEC)*, pp. 2184-2191, 2014.

[24] G. Shen, D. Xu, L. Cao, and X. Zhu, "An improved control strategy for grid-connected voltage source inverters with a LCL filter," *IEEE Trans. Power Electron.*, Vol. 43, No. 5, pp. 1899-1906, Jul. 2008.

[25] L. D. Zhang, "Interconnection of two very weak AC systems by VSC-HVDC links using power-synchronization control," IEEE Trans. Power Syst., Vol. 26, No. 1, pp. 344-355, Feb. 2011.

Jian-jun Sun was born in China. He received his Ph.D. degree in Electrical Engineering from Wuhan University, Wuhan, China, in 2007. He is presently working as an Assistant Professor in the School of Electrical Engineering, Wuhan University. His current research interests include the analysis and control of power electronics systems, power

quality control and the modeling and analysis of microgrids.

Wei Hu was born in China. She received her Ph.D. degree in Electrical Engineering from Wuhan University, Wuhan, China, in 2015. She is presently working in the Grid Center Department, State Grid Hubei Electric Power Research Institute, Wuhan, China. Her current research interests include microgrid stability, microgrid power quality and the control and protection of DC transmissions.

Hui Zhou was born in China, in 1990. He received his B.S. degree in Electrical Engineering from Wuhan University, Wuhan, China, in 2013; where he is presently working towards his M.S. degree. His current research interests include power quality, microgrid stability analysis and the control of power electronic converters.

Yi-ming Jiang was born in China, in 1990. He received his B.S. degree in Electrical Engineering from Wuhan University, Wuhan, China, in 2013; where he is presently working towards his M.S. degree. His current research interests include micro-grid stability analysis and the control of power electronic converters.

Xiao-ming Zha received his B.S., M.S. and Ph.D. degrees in Electrical Engineering from Wuhan University, Wuhan, China, in 1989, 1992 and 2001, respectively. Since 1992, he has been a Faculty Member in the School of Electrical Engineering, Wuhan University, where he is presently working as a Professor. From October 2001 to February 2003, he was a Postdoctoral Fellow with the University of Alberta, Edmonton, AB, Canada. His current research interests include medium-voltage motor drives, apparatus for power quality control, static synchronous compensators, and application technologies for the renewable energy resources in micro-grids.